nature energy

Supplementary information https://doi.org/10.1038/s41560-026-02122-6

Heat-driven elastocaloric cooling with shape memory films

In the format provided by the authors and unedited

Table of contents

Supplementary Notes

Supplementary Note 1. Detailed calculation of the force–displacement ratio of actuators.

The force–displacement ratio of an actuator is defined as the ratio between the maximum output force and the stroke length:

$$\text{Force–displacement ratio} = \frac{\text{maximum output force (N)}}{\text{maximum stroke length (mm)}} \qquad (S1)$$

The target force–displacement ratio in this work was determined based on the mechanical loading requirements of the refrigerant film. Specifically, a transformation force of 5–6 N and a corresponding linear displacement of 300–375 μm (equivalent to 4–5% strain) are required to fully drive the phase transformation. This results in a target force–displacement ratio of 16.0−16.7 N mm^{-1}.

For the SMA-based thermal actuator developed in this work, the maximum output force when coupled with the refrigerant film is approximately 5.5 N, and the maximum stroke is approximately 0.38 mm, corresponding to a force–displacement ratio of 14.5 N mm^{-1}. The experimentally achieved force–displacement ratio of the thermal actuator is in good agreement with the target value, confirming that the actuator provides sufficient mechanical output to drive the refrigerant film.

For comparison, the force–displacement characteristics of a commercial electromechanical actuators from ESR Pollmeier GmbH used in this study were analyzed. The actuator provides a maximum continuous force of 116 N and a stroke of 106 mm[1], corresponding to a force–displacement ratio of approximately 1.1 N mm^{-1}.

Supplementary Note 2. Detailed calculation of coefficient of performance (COP) and exergetic efficiency.

The coefficient of performance (COP) and exergetic efficiency (η_{ex}) are evaluated under different input-power definitions to provide a comprehensive assessment of system performance. The COP is defined as the ratio of cooling output to input energy and is not bounded by unity, whereas η_{ex} is normalized with respect to the corresponding Carnot limit and is therefore bounded by 100%.

In addition to calculations based solely on actuator thermal input, we further consider (i) electrical power supplied for Joule heating (ii) input power required to maintain the external heat source, and (iii) electrical power consumed by the two auxiliary linear actuators used to cyclically move the heat exchangers.

When electrical input power for Joule heating is used as the basis, a significant fraction of the supplied energy is dissipated to the surroundings as waste heat, reducing overall system efficiency. Under this definition, the full-system COP of the Joule-heated configuration decreases from 8.53×10^{-2} (thermal input basis) to 2.18×10^{-2} (electrical input basis), and the corresponding exergetic efficiency decreases from 7.27×10^{-2} % to 1.86×10^{-2} %. Similarly, the thermal actuator COP decreases from 3.27×10^{-2} to 8.37×10^{-3}, and its exergetic efficiency decreases from 3.27% to 0.837 %.

For the externally heat-driven configuration, the temperature evolution of the actuator film cannot be directly monitored by infrared imaging due to geometric constraints. When the input power required to maintain the external heat-source is used as the system input, the full-system COP decreases to 3.63×10^{-3} (temperature-slope method) and 5.60×10^{-3} (counter-heating method). The corresponding heat-driven actuator COP is 2.43×10^{-3}. The full-system and actuator exergetic efficiencies are 2.16×10^{-3} % and 0.243 %, respectively.

The electrical power consumption of the auxiliary linear actuators accounts for more than 90% of the total electrical input power in the present laboratory prototype. This is primarily due to the use of high-precision servo actuators selected to enable accurate control and a wide operating range during initial prototyping. When auxiliary actuator consumption is included, the full-system COP of the Joule-heated configuration decreases to 6.69×10^{-4}, with a corresponding exergetic efficiency of 5.71×10^{-4} %. For the externally heat-driven configuration, the full-system COP decreases to 3.17×10^{-4} and the exergetic efficiency to 1.22×10^{-4} %. These values reflect the experimental hardware configuration rather than intrinsic limitations of the heat-driven elastocaloric concept. In practical implementations, replacing the laboratory servo actuators with compact, low-power actuators would substantially reduce total electrical input and improve overall system efficiency.

A complete summary of COP and exergetic efficiencies under all evaluation criteria is provided in Supplementary Table 4. Below we provide detailed formulations for the corresponding calculations.

Coefficient of performance (COP)

The coefficient of performance (COP) is defined as:

$$COP = \frac{\dot{Q}_c}{\dot{W}_{in}} \tag{S2}$$

where $\dot{Q}_c$ is the cooling power and $\dot{W}_{in}$ is the average input power over one cycle under the specified evaluation condition.

1. Full coupled heat-driven system

1.1 Thermal input basis

Under the thermal input basis, the input power is defined as the thermal energy absorbed by the actuator film during heating, divided by the cycle time:

$$\dot{W}_{in,thermal} = \frac{m_{act} c_{p,act} \Delta T_{act}}{T} \tag{S3}$$

where m_{act} is the mass of the actuator film, $c_{p,act}$ is the specific heat capacity of the actuator material, ΔT_{act} is the measured temperature rise of the actuator film during heating, and T is the cycle time.

This definition corresponds to the "Full system (thermal input basis)" in Supplementary Table 4.

1.2. Electrical input basis (Joule-heated actuation)

When Joule heating is used, the electrical power supplied to the actuator film is taken as the input:

$$\dot{W}_{in,Joule} = \frac{1}{T}\int_0^T v(t) \cdot i(t)\, dt \tag{S4}$$

where T is the cycle time, and $v(t)$ and $i(t)$ are the instantaneous input voltage and current applied to the actuator film during the cycle.

This corresponds to "Full system (electrical input basis, Joule-heated actuation)" in Supplementary Table 4.

1.3. Electrical input basis (external heat-source actuation)

For externally heat-driven operation, the input power required to maintain the external heat source temperature is taken as system input:

$$\dot{W}_{in,HS} = \frac{1}{T}\int_{t_1}^{t_2} V \cdot I\, dt \tag{S5}$$

where T is the cycle time, V and I are the average voltage and current supplied to the heat source, and t_1 to t_2 corresponds to the duration of contact between the actuator film and the heat source during each cycle.

This corresponds to "Full system (electrical input basis, external heat-source actuation)" in Supplementary Table 4.

1.4. Full system including auxiliary actuators

When the electrical power consumption of the two auxiliary linear actuators used to move the heat exchangers is included, the total input power becomes:

$$\dot{W}_{\text{in,total}} = \dot{W}_{\text{in,Joule/HS}} + \dot{W}_{\text{aux}} \quad (S6)$$

The auxiliary actuator contribution is calculated as:

$$\dot{W}_{\text{aux}} = \frac{1}{T}\left(\int_{loading} P_{\text{aux}}(t)\,dt + \int_{unloading} P_{\text{aux}}\,(t)dt\right) \quad (S7)$$

where $P_{\text{aux}}\,(t)$ is the instantaneous electrical power of the two auxiliary actuators. Only the loading and unloading intervals are considered.

This definition corresponds to "Full system (+ auxiliary actuators)" in Supplementary Table 4.

In the present laboratory prototype, auxiliary actuator consumption accounts for more than 90% of the total electrical input power due to the use of high-precision servo actuators selected for experimental control. These values reflect the prototyping configuration rather than representing an intrinsic thermodynamic limitation of thermally driven elastocaloric cooling.

2. Sub systems

2.1 Elastocaloric cooling unit

Without work recovery (WR):

$$\dot{W}_{\text{in,Cooler,woWR}} = f \cdot \int_{\text{loading}} Fdx \quad (S8)$$

With work recovery:

$$\dot{W}_{\text{in,Cooler,wiWR}} = f \cdot \oint Fdx = f \cdot \left(\int_{\text{loading}} Fdx + \int_{\text{unloading}} Fdx\right) \quad (S9)$$

where f is the operating frequency. In the present prototype, work recovery is not implemented due to the one-way SMA actuator configuration. COP values with work recovery therefore represent a theoretical upper bound for benchmarking future bidirectional actuator designs.

2.2 Thermal actuation unit

The thermal actuator efficiency is defined as

$$COP_{\text{actuator}} = \frac{\dot{W}_{\text{act,woWR}}}{\dot{W}_{\text{in}}} \quad (S10)$$

where the mechanical work output of the actuator without work recovery is:

$$\dot{W}_{\text{act,woWR}} = f \cdot \int_{\text{loading}} Fdx \quad (S11)$$

Here, F and x correspond to the measured force and coupled displacement used in the force–stroke loop. The "loading" branch refers to the actuation/loading stage only (no work recovery).

For the Joule-heated configuration, the input power $\dot{W}_{\mathrm{in}}$ is $\dot{W}_{\mathrm{in,thermal}}$ under the thermal-input basis, or $\dot{W}_{\mathrm{in,Joule}}$ under the electrical-input basis. For the externally heat-driven configuration, the input power $\dot{W}_{\mathrm{in}}$ is $\dot{W}_{\mathrm{in,HS}}$.

Exergetic efficiency

The exergetic efficiency is defined as:

$$\eta_{\mathrm{ex}} = \frac{\dot{Q}_{\mathrm{c}}\left(\frac{T_0}{T_{\mathrm{c}}} - 1\right)}{\dot{Q}_{\mathrm{h}}\left(1 - \frac{T_0}{T_{\mathrm{s}}}\right)} \qquad (S12)$$

where T_0 is the ambient temperature, T_{c} is the heat-source temperature in the cooling unit, and T_{s} is the actuator temperature (Joule-heated case) or external heat-source temperature. The corresponding values of T_0, T_{c}, and T_{s} under different operating conditions are provided in Supplementary Table 4. $\dot{Q}_{\mathrm{h}}$ is the input power term consistent with the selected evaluation basis.

For consistency with COP definitions:

Under the thermal-input basis:

$$\dot{Q}_{\mathrm{h}} = \dot{W}_{\mathrm{in,thermal}} \qquad (S13)$$

Under the electrical input basis for Joule-heated actuation:

$$\dot{Q}_{\mathrm{h}} = \dot{W}_{\mathrm{in,Joule}} \qquad (S14)$$

Under the electrical input basis for external heat-source actuation:

$$\dot{Q}_{\mathrm{h}} = \dot{W}_{\mathrm{in,HS}} \qquad (S15)$$

When the auxiliary actuators are additionally included:

$$\dot{Q}_{\mathrm{h}} = \dot{W}_{\mathrm{in,total}} \qquad (S16)$$

The actuator exergetic efficiency is obtained by taking its mechanical work output (without WR) as useful output and the corresponding input power as $\dot{Q}_{\mathrm{h}}$.

Supplementary Note 3. Detailed calculation of thermal time constant for heat transfer between refrigerant film and heat sink/source.

The heat-transfer pathway is schematically illustrated in Supplementary Fig. 16a. During operation, heat flows from the refrigerant film through the solid–solid contact interface to the copper heat sink or heat source when mechanical pressure is applied.

The overall thermal resistance consists of three components: the internal resistance of the refrigerant film ($R_{\mathrm{refrigerant}}$), the interfacial contact resistance (R_{contact}), and the internal resistance of the Cu heat exchanger (R_{Cu}). Due to the small thickness and relatively high thermal conductivity of both the refrigerant film and the Cu heat exchanger, their internal thermal resistances are negligible compared to the interfacial resistance. Therefore, the lumped-capacitance approximation is applicable.

The validity of lumped system analysis is assessed using the Biot number:

$$Bi = \frac{h_{\mathrm{contact}} L_c}{k} \tag{S17}$$

where h_{contact} is the interfacial thermal conductance, k is thermal conductivity, and L_{c} is the characteristic length. When $Bi << 0.1$, spatial temperature gradients within the solid are negligible.

Under this assumption, the thermal time constant τ of the refrigerant film is given by:

$$\tau = \frac{\rho_{\mathrm{refrigerant}}\, L_{\mathrm{c,refrigerant}}\, c_{\mathrm{p,refrigerant}}}{h_{\mathrm{contact}}} \tag{S18}$$

where $\rho_{\mathrm{refrigerant}}$ is density, $c_{\mathrm{p,refrigerant}}$ is specific heat capacity, and $L_{\mathrm{c,refrigerant}}$ is the characteristic length.

Typical interfacial conductance values for solid–solid contact under moderate pressure range from 1000 to 3000 W/m^2 K. Using these values yields a theoretical thermal time constant in the range of 28–84 ms.

The temperature evolution of the heat sink and heat source in the Joule-heated configuration (0.83 Hz frequency, 500 ms contact time) is shown in Supplementary Fig. 16b. The heat sink approaches thermal equilibrium after approximately 270 ms ($t_{\mathrm{heat,0}}$ to $t_{\mathrm{heat,1}}$), while the heat source requires approximately 350 ms ($t_{\mathrm{cool,0}}$ to $t_{\mathrm{cool,1}}$). Effective heat transfer therefore occurs within the available 500 ms contact duration.

A first-order thermal system reaches more than 99% equilibrium after approximately 5τ. Based on the experimentally observed equilibrium time of ~310 ms, the corresponding time constant is:

$$\tau \approx 62 \text{ ms}$$

Using this experimentally derived time constant, the effective interfacial conductance is calculated as:

$$h_{\mathrm{contact}} \approx 1350 \text{ W/m}^2 \text{ K}$$

This value falls within the expected range for solid–solid interfaces under moderate pressure, confirming consistency between theoretical estimation and experimental observation.

The parameters used in the above calculations are summarized below.

Parameter	Definition	Value	Unit
$L_{\text{c,refrigerant}}$	Characteristic length of refrigerant film	26×10^{-6} **	m
$L_{\text{c,Cu}}$	Characteristic length of Cu heat sink/source	100×10^{-6} **	m
$k_{\text{refrigerant}}$	Thermal conductivity of refrigerant film	18 *	W/m K
k_{Cu}	Thermal conductivity of Cu heat sink/source	400 *	W/m K
h_{contact}	Interfacial conductance	1350	W/m^2 K
$Bi_{\text{refrigerant}}$	Biot number of refrigerant film	0.0020	–
Bi_{Cu}	Biot number of Cu heat sink/source	0.0003	–
$\rho_{\text{refrigerant}}$	Density of refrigerant film	6460 ***	Kg/m^3
$c_{\text{p,refrigerant}}$	Specific heat capacity of refrigerant film	500	J/kg K

*   Values obtained from literature (see Ref. 2)

** Experimental measured values

*** Calculated from nominal atomic composition using atomic weights from Ref. 2.

Supplementary Figures

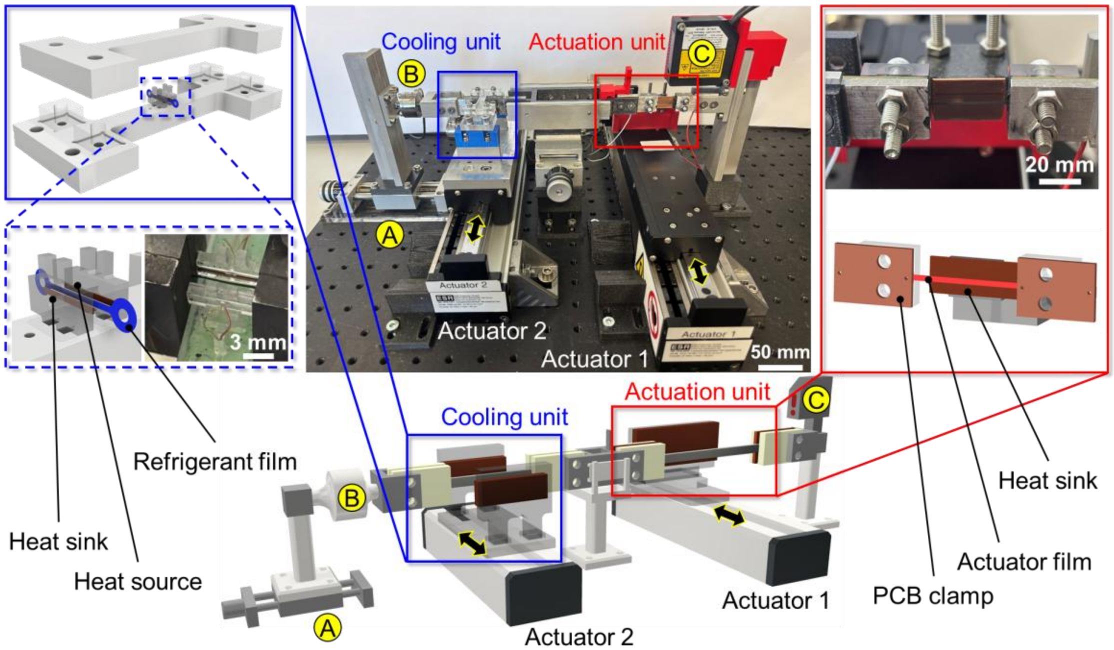

Supplementary Fig. 1. Detailed illustration of the film-based heat-driven elastocaloric cooling prototype. Top center: Photograph of the integrated prototype comprising the thermal actuation unit (right) and the cooling unit (left). Bottom center: Simplified schematic representation highlighting the arrangement of key components. Top left inset: Enlarged view of the cooling unit, consisting of a Cu heat sink and heat source supported by PMMA structures, with the refrigerant film positioned in between. Top right inset: Enlarged view of the thermal actuation unit, where the actuator film is clamped using a PCB board and PMMA block to provide mechanical fixation and electrical connection. Thermal input can be supplied either by Joule heating or by an external heat source. A Cu sheet heat sink is mounted on an electromechanical actuator via a 3D-printed cantilever beam to remove heat from the actuator during recovery. Labels: (A) linear stage for pre-straining, (B) force sensor, (C) laser displacement sensor.

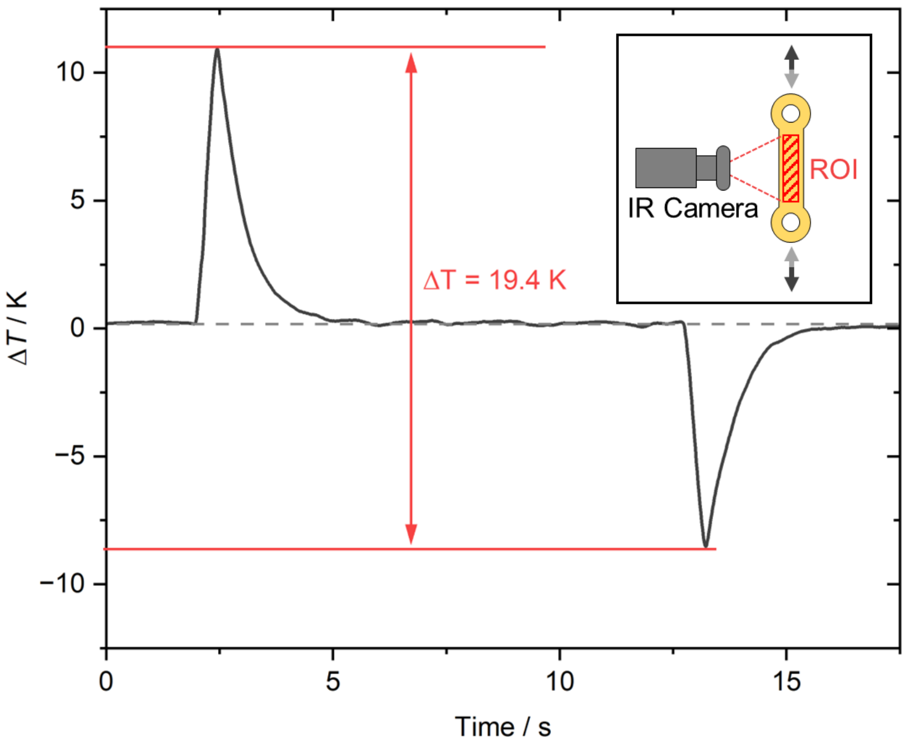

Supplementary Fig. 2. Adiabatic temperature change of superelastic TiNiFe film. Infrared (IR)-thermography measurement shows an average adiabatic temperature change (ΔT) of 19.4 K under a strain rate of 0.1 s^{-1} at 5.2% strain. The TiNiFe film was uniaxially loaded and unloaded using a tensile testing machine, while temperature was recorded over the central area as the region of interest (ROI), as illustrated in the inset schematic.

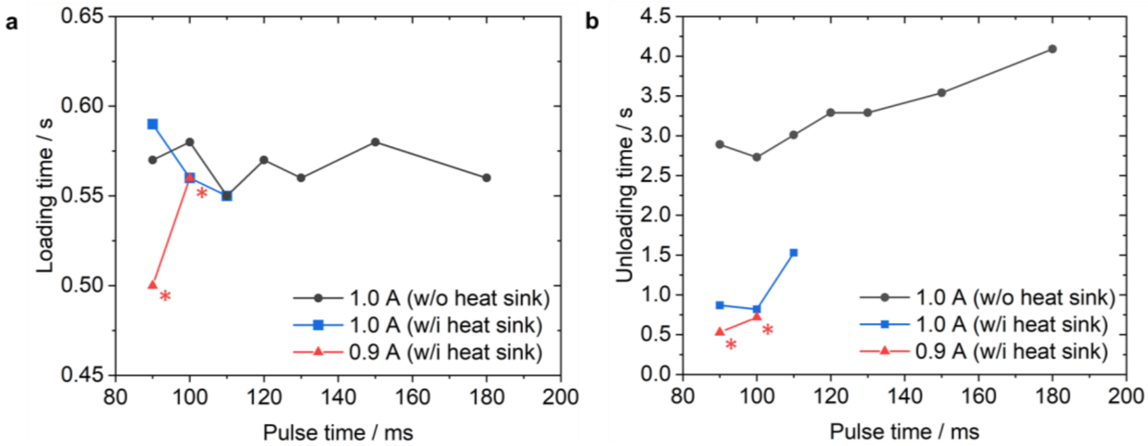

Supplementary Fig. 3. Loading and unloading times of the Joule-heated thermal actuator film. a, Loading time remains above 0.5 s and shows no clear dependence on pulse duration. The shortest loading time of 500 ms was achieved with a 0.9 A heating current and a 90 ms pulse. **b,** Unloading time remains above 2.5 s without a heat sink. Incorporating a heat sink significantly reduces unloading time to below 1.0 s at shorter pulse durations. The shortest unloading time achieved was 530 ms under 0.9 A heating current and 90 ms pulse. Data marked with * were obtained with a 24 mm-long actuator film pre-strained by 770 µm, while other data were measured with a 19 mm-long film pre-strained by 520 µm. Symbols represent experimental data, and lines are guides to the eye.

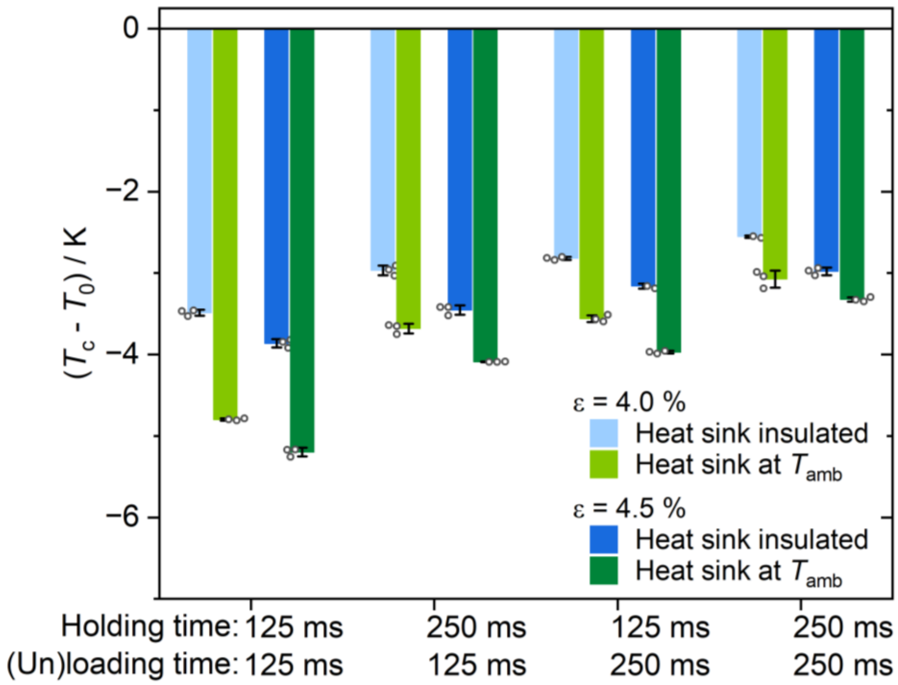

Supplementary Fig. 4. Comparison of temperature drop (T_c – T_0) under different heat-sink boundary conditions and strain ε. Temperature drops were measured using the stand-alone cooling unit driven by electromechanical actuators. Results are shown for ε = 4% and ε = 4.5% at different (un)loading and holding times (125 ms and 250 ms). Light blue and dark blue bars represent ε = 4% and ε = 4.5%, respectively, with the heat sink insulated. Light green and dark green bars represent ε = 4% and ε = 4.5%, respectively, with the heat sink maintained at ambient temperature (T_{amb}). Maintaining the heat sink near ambient temperature using a larger thermal mass (limiting the hot-side temperature rise to <1 K above ambient) increases the temperature drop by an average of 0.8 K compared to the insulated condition. Detailed numerical values are provided in Supplementary Table 1. Data are shown as mean ± standard deviation (n = 3 independent experiments, labeled as dots).

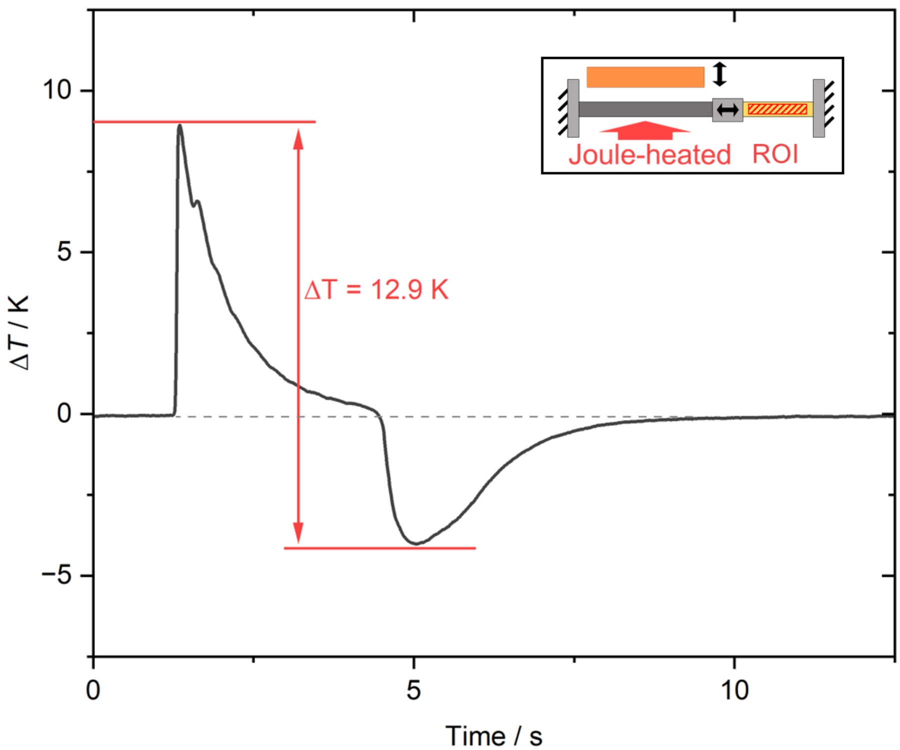

Supplementary Fig. 5. IR-thermography of the refrigerant film under Joule-heated actuation. The thermal actuator, activated by an electrical pulse train, loads the TiNiFe refrigerant film into the stress-induced martensite state and holds for 3 s before unloading. A maximum material-level temperature change of 12.9 K is observed under quasi-adiabatic conditions. This value does not correspond to the fully adiabatic temperature change of 19.4 K measured independently under high strain-rate tensile testing (Supplementary Fig. 2). The temperature rise during loading exceeds the temperature drop during unloading due to the higher loading strain rate (0.09 s^{-1}) compared to the unloading strain rate (0.03 s^{-1}), as well as asymmetric thermal time constants governing heat exchange with the surroundings.

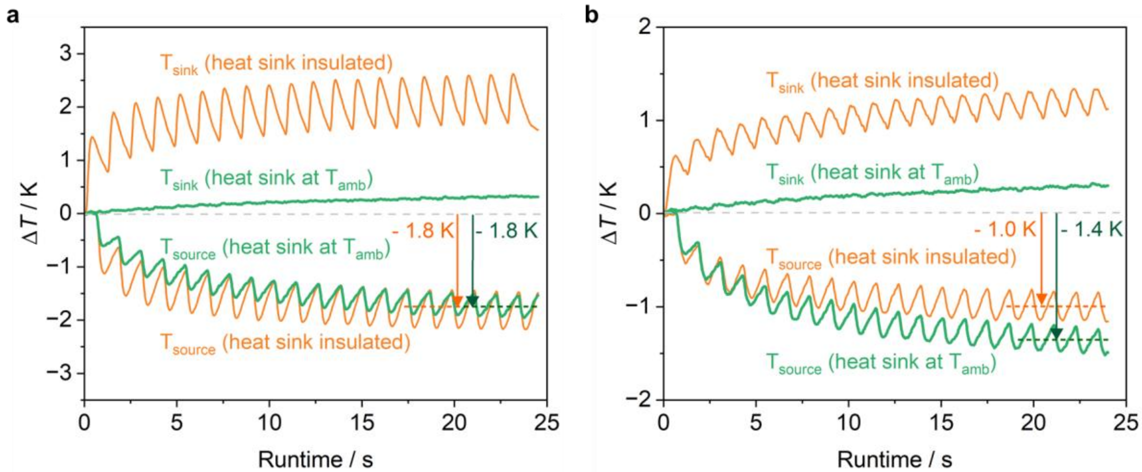

Supplementary Fig. 6. Effect of heat-sink boundary conditions on temperature drop ($T_c - T_0$) for (a) Joule-heated and (b) externally heat-driven elastocaloric devices. a, In the Joule-heated actuation configuration, the temperature drop remains unchanged at −1.8 K whether the heat sink is insulated or maintained near ambient temperature. **b,** In the externally heat-driven configuration, maintaining the heat sink near ambient temperature increases the temperature drop from −1.0 K (insulated) to −1.4 K. In both panels, orange curves correspond to the insulated heat-sink condition, and green curves correspond to the heat sink maintained near ambient temperature.

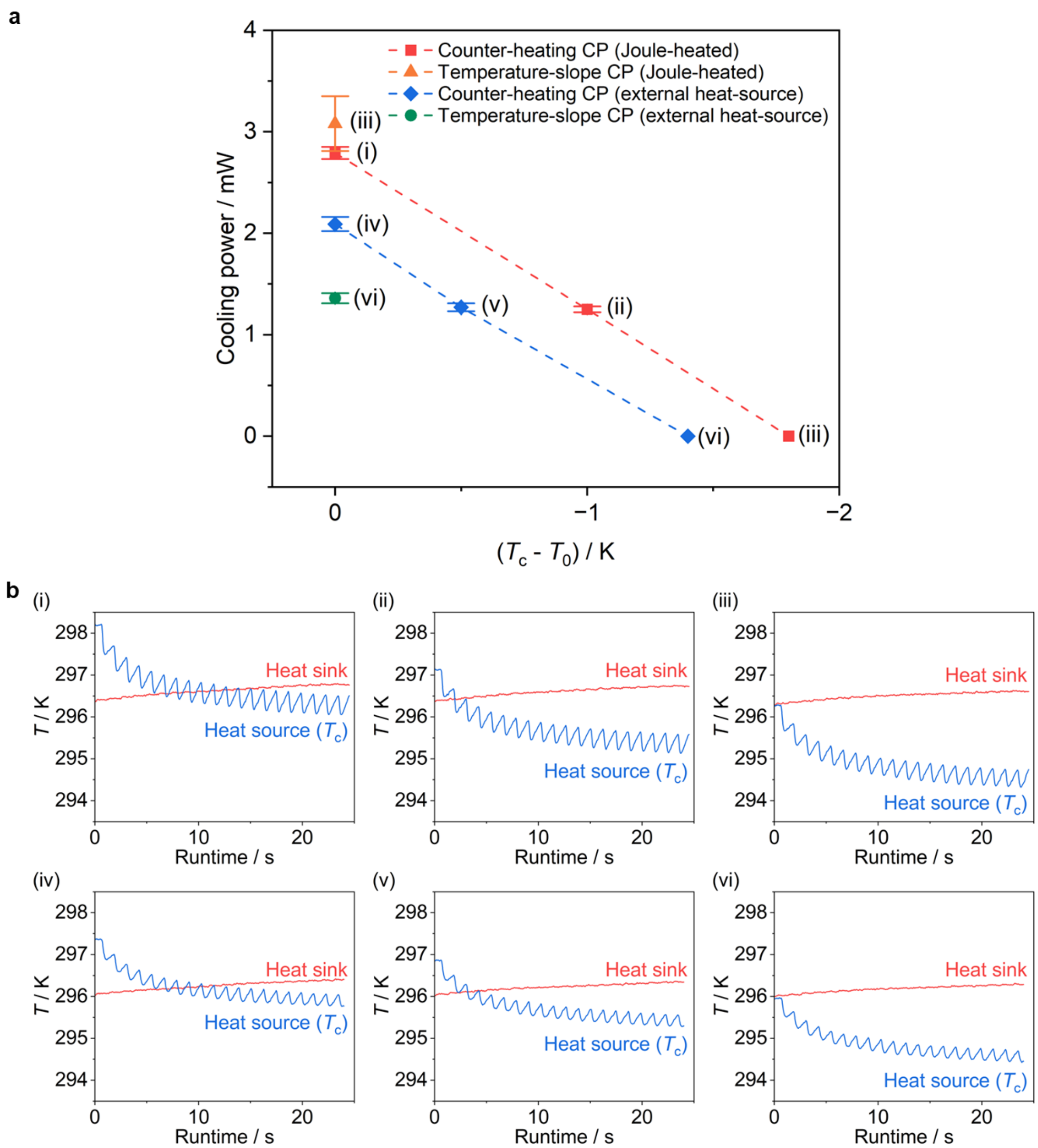

Supplementary Fig. 7. Cooling power under different actuation modes and determination methods. a, Cooling power values for the Joule-heated actuation configuration are shown in red (counter-heating method) and orange (temperature-slope method). Cooling power values for the external heat-source actuation configuration are shown in blue (counter-heating method) and green (temperature-slope method). Cooling power determined using the temperature-slope method is derived from the initial temperature decay rate of the heat source during the first cooling cycle at zero temperature lift. Cooling power determined using the counter-heating method is obtained by supplying electrical power through a calibrated resistance wire to offset the cooling effect. The parameters used in the temperature-slope analysis are listed in Supplementary Table 2, and detailed numerical values of cooling power are provided in Supplementary Table 3. Labels (i)−(vi) correspond to the transient temperature evolution under different external thermal loads shown in panel **b**. Data are presented as mean ± standard deviation (n = 3 independent experiments). Symbols represent experimental data points, and dashed lines serve as guides to the eye. **b,** Transient evolution of temperature under different external thermal loads. Red curves represent the temperature of the heat sink which remains close to ambient temperature, while blue curves represent the temperature of the heat source (T_c). In the counter-heating measurements, the heat source is preheated using a resistance wire to establish a controlled thermal load, after which the elastocaloric system is activated while the electrical heating is maintained to reach steady-state conditions. In cooling power calculation of temperature-slope method, the initial cooling rate of transient temperature profiles in (iii) and (vi) are used.

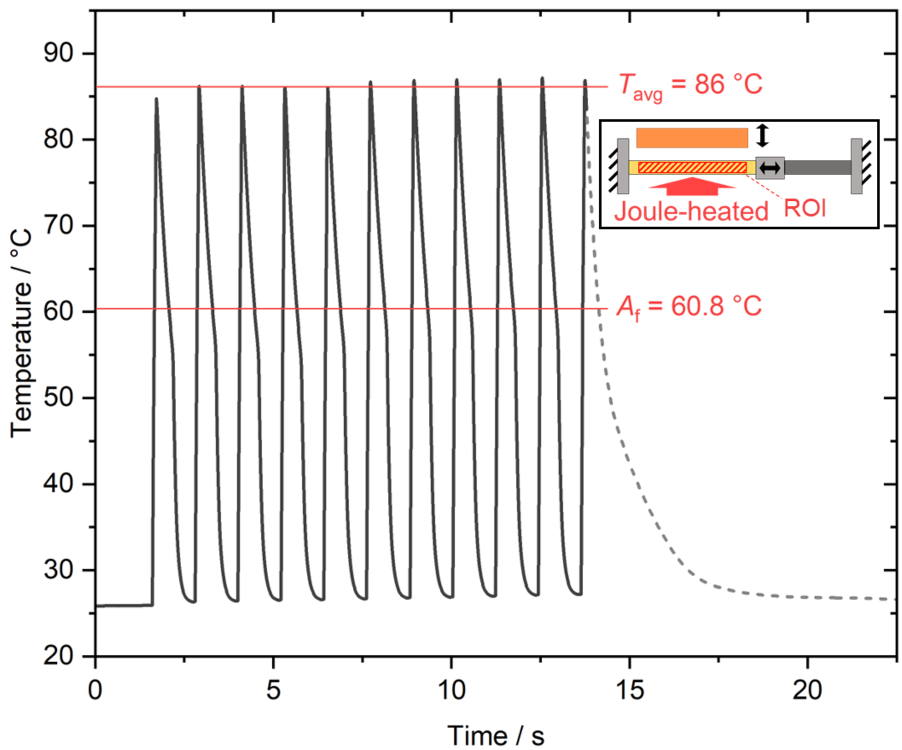

Supplementary Fig. 8. IR-thermography of the thermal actuator film under Joule-heated cyclic operation. The actuator film is cyclically activated by Joule heating, with an electrical current of 1.0 A and a pulse time of 100 ms applied every 1.2 s. The film reaches an average temperature of 86 °C, as measured by IR thermography in the selected ROI (inset), exceeding the austenite finish temperature (A_f = 60.8 °C) and thereby driving the martensite-to-austenite phase transformation required for actuation.

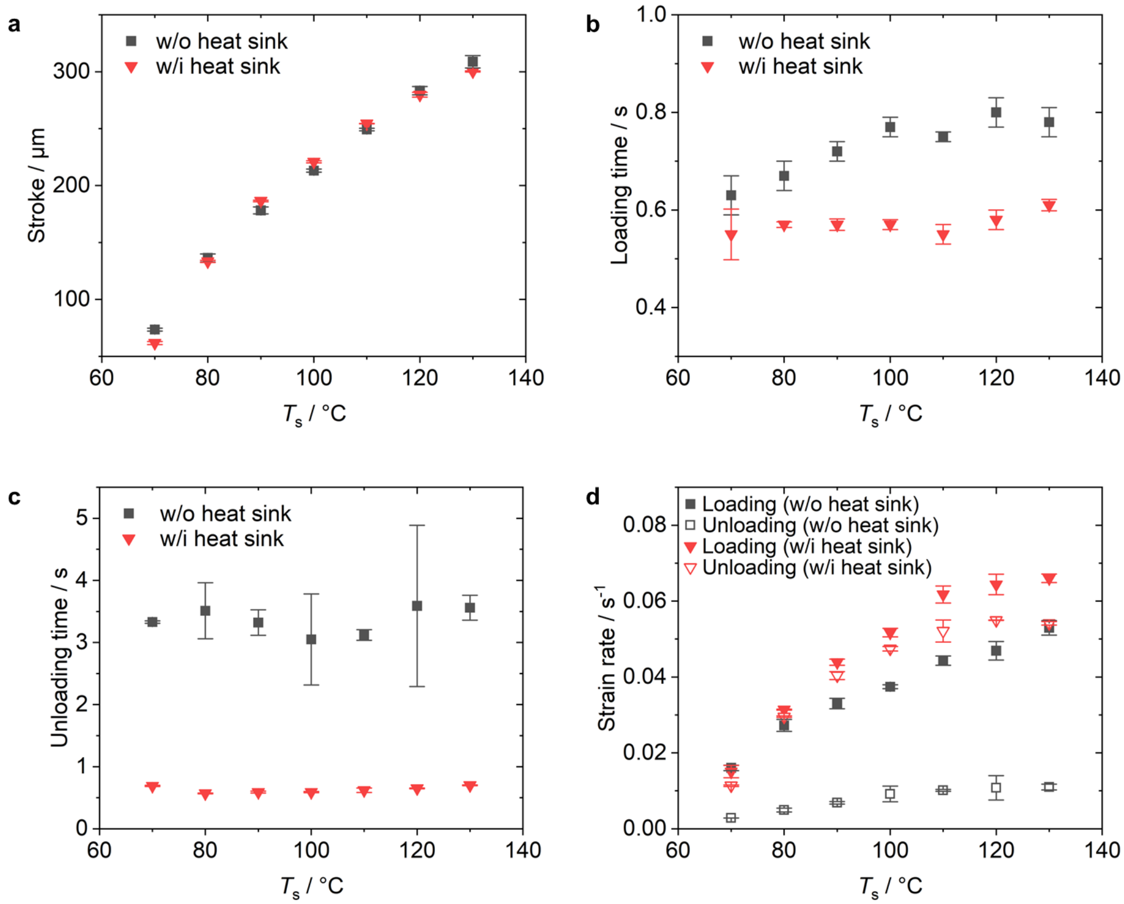

Supplementary Fig. 9. Performance of the external heat-source actuation unit at heat-source temperatures from 70 to 130 °C with a 250 ms contact time. Data obtained without and with implementation of the heat sink are shown in black and red, respectively. **a,** Actuation stroke as a function of heat-source temperature (T_s). At 130 °C, strokes exceed 300 μm for both configurations, providing sufficient strain to load the refrigerant film. **b,** Loading time versus T_s. Without active heat-sink implementation, loading times range from approximately 0.6 to 0.8 s. Incorporating active heat-sink movement reduces the loading time to 0.6 s and improves consistency. **c,** Unloading time versus T_s. In the absence of an active heat sink, the actuator film dissipates heat directly to the ambient air without solid–solid thermal contact. Under these conditions, unloading times exceeds 3 s and exhibit significant variability due to uncontrolled convective cooling. With active heat-sink implementation, unloading time is constrained to 0.6 s, markedly improving repeatability. **d,** Corresponding strain rates during loading and unloading. Active heat-sink control increases both loading and unloading strain rates, approaching the adiabatic regime, reaching 0.07 s^{-1} (loading) and 0.05 s^{-1} (unloading) at 130 °C. Data are shown as mean ± standard deviation (n = 3 independent experiments).

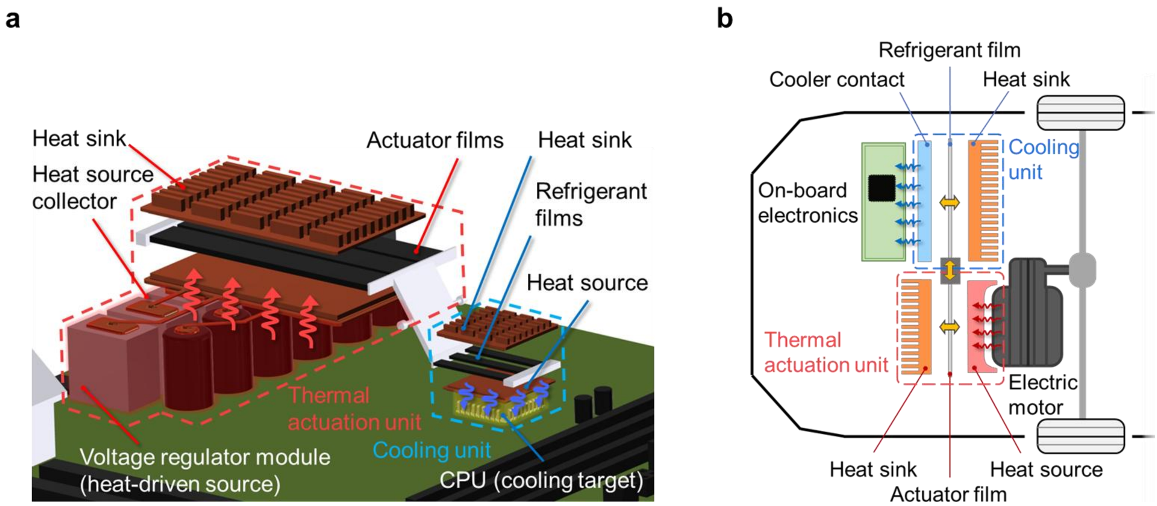

Supplementary Fig. 10. Potential applications of film-based heat-driven elastocaloric cooler. a, Application concept in computers: waste heat from the voltage regulator module (VRM), which can reach up to ~85 °C under normal load, can serve as the heat source to drive the thermal actuation unit. The generated mechanical work can then power the elastocaloric cooling unit for active cooling of the CPU. **b,** Application concept in electric vehicles (EVs): waste heat from the electric motor, which can exceed 100 °C during operation, can be harvested to drive the heat-driven elastocaloric cooler. This provides active cooling for on-board electronics or power electronics, enhancing thermal management in EV systems.

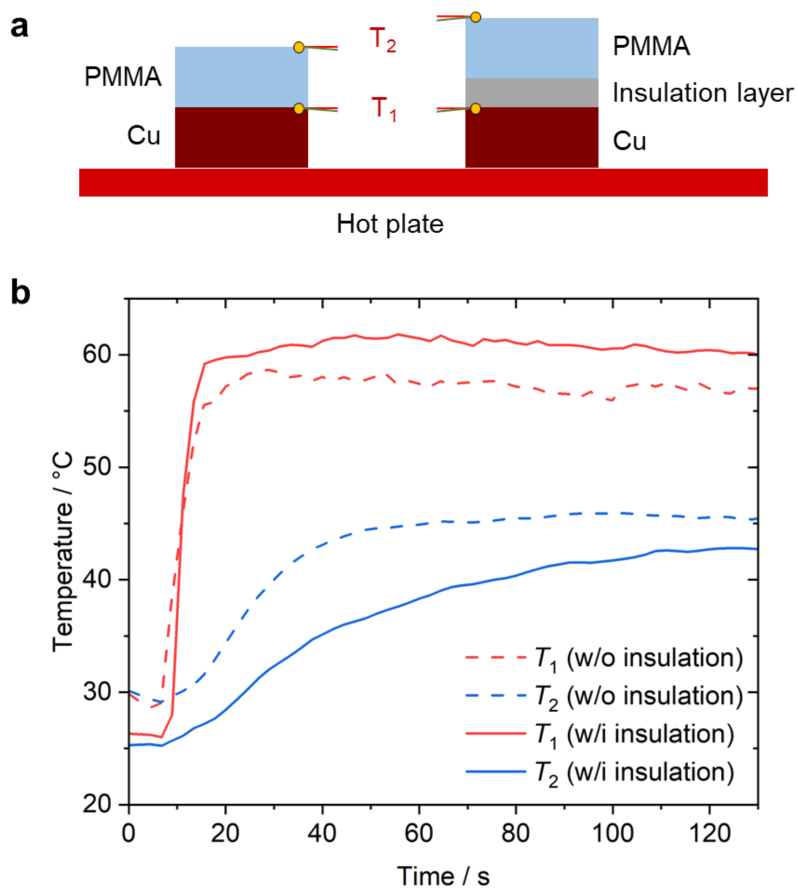

Supplementary Fig. 11. Effect of aerogel thermal insulation layer. a, Schematic of the testing setup for evaluating a 350 μm thick aerogel thermal insulation layer. A Cu sheet was heated by direct contact with a hot plate. Thermocouple T_1 was positioned on top of the Cu sheet and covered by a PMMA board, while thermocouple T_2 was placed on top of the PMMA board. To test the insulation performance, the aerogel layer was inserted between the Cu sheet and the PMMA board, with T_1 located beneath the insulation layer. **b,** Temperature evolution of T_1 and T_2 with and without the aerogel insulation layer. Results show that the insulation layer effectively reduces heat transfer from the Cu sheet, lowering T_2 and stabilizing the temperature gradient.

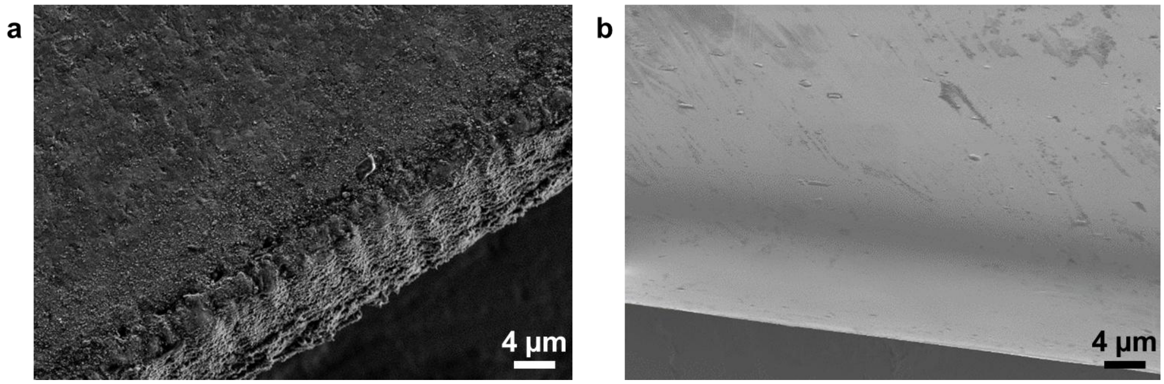

Supplementary Fig. 12. Scanning electron microscope (SEM) images of TiNiFe refrigerant film. a, SEM image of the film edge after ultra-short pulse laser cutting, showing rough morphology with cutting-induced surface features. **b,** SEM image of the film edge after electropolishing, revealing a smooth and defect-free surface finish compared to the as-cut state.

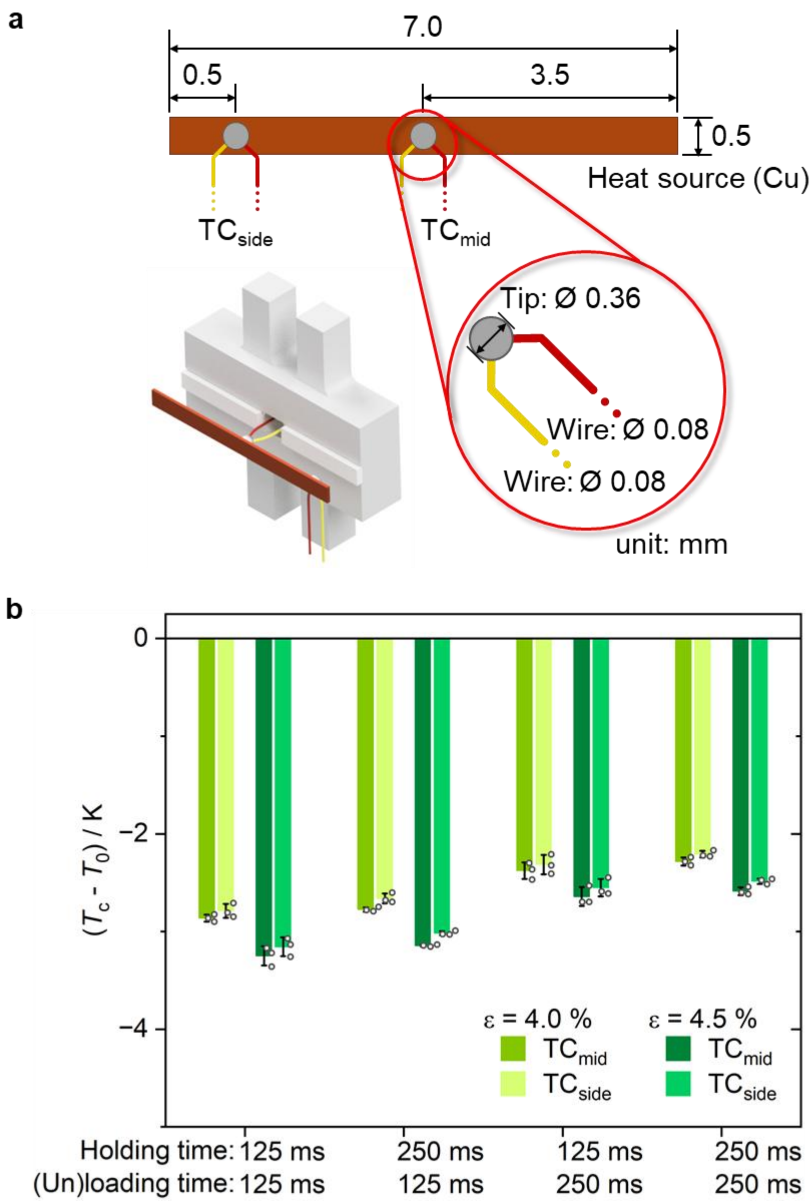

Supplementary Fig. 13. Validation of thermocouple measurement positions at the heat source in the cooling unit. a, Schematic illustration of the heat-source geometry (dimensions in mm) and thermocouple measurement locations. All device-level temperatures reported in the cooling unit are measured at the center of the heat source (TC_{mid}). An additional thermocouple (TC_{side}) was positioned near the edge of the heat source to verify spatial temperature uniformity. **b,** Comparison of temperature differences ($T_c - T_0$) are measured at TC_{mid} and TC_{side} under 4% and 4.5% strain conditions using electromechanical actuation. The temperature difference between the two measurement positions remains below 0.1 K for all tested conditions, confirming a homogeneous temperature distribution across the heat source and validating the use of TC_{mid} as a representative measurement point. Detailed numerical values are provided in Supplementary Table 1. Data are presented as mean ± standard deviation (n = 3 independent experiments, labeled as dots).

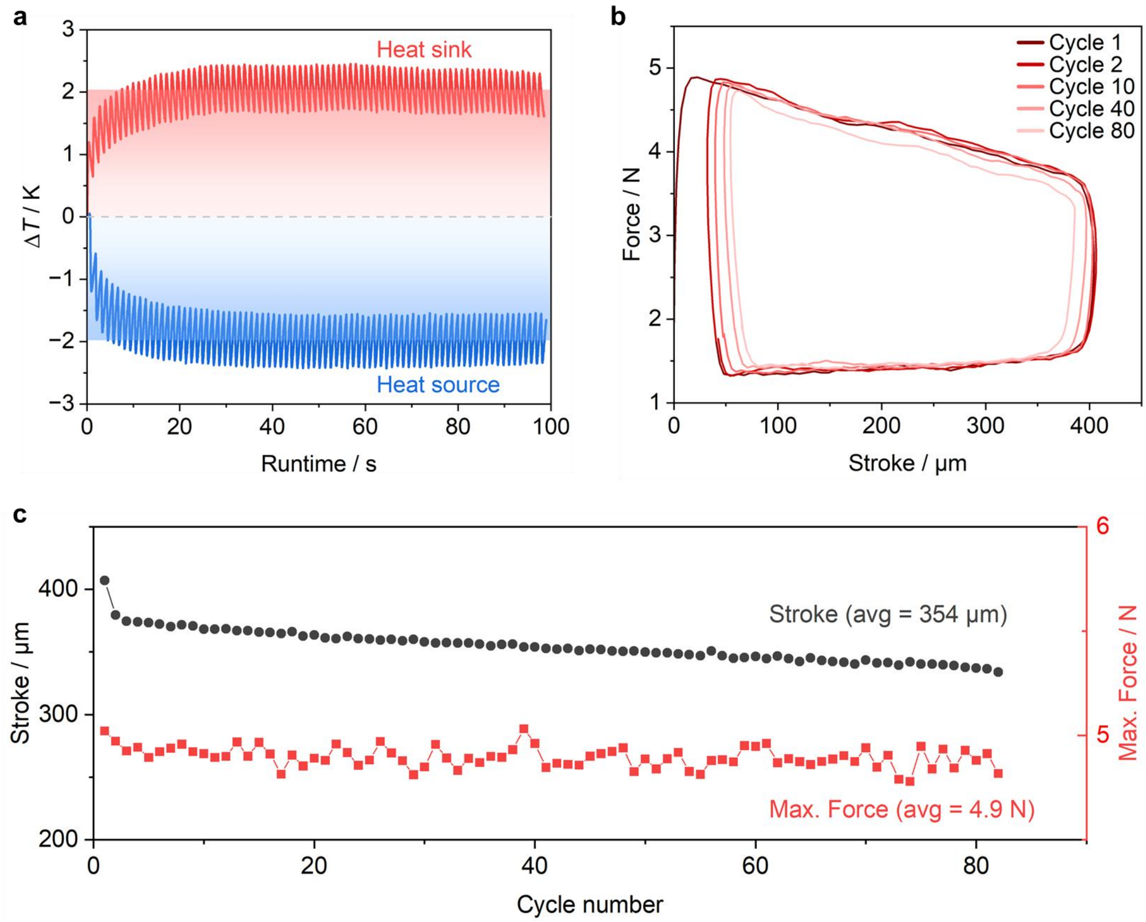

Supplementary Fig. 14. Stability of the Joule-heated heat-driven elastocaloric cooling system over 80 cycles. a, Device-level temperature span (ΔT) during 80 consecutive cycles (96 s) at 0.83 Hz, showing a stable steady-state span of approximately 4.0 K. **b,** Force–stroke hysteresis loops of the coupled actuator–refrigerant system at selected cycles (1, 2, 10, 40, and 80), demonstrating reproducible mechanical response during cyclic operation. A moving average of 6 data points was applied for readability. **c,** Cycle-resolved actuation stroke and maximum force. The stroke exhibits an initial decrease after the first cycle followed by gradual stabilization, with an average value of 354 μm and a minimum value above 330 μm, remaining above the design threshold of 300 μm throughout the test. The maximum force remains stable with an average of 4.9 N, indicating sustained mechanical loading capability of the refrigerant film. Symbols represent experimental data; lines are guides to the eye.

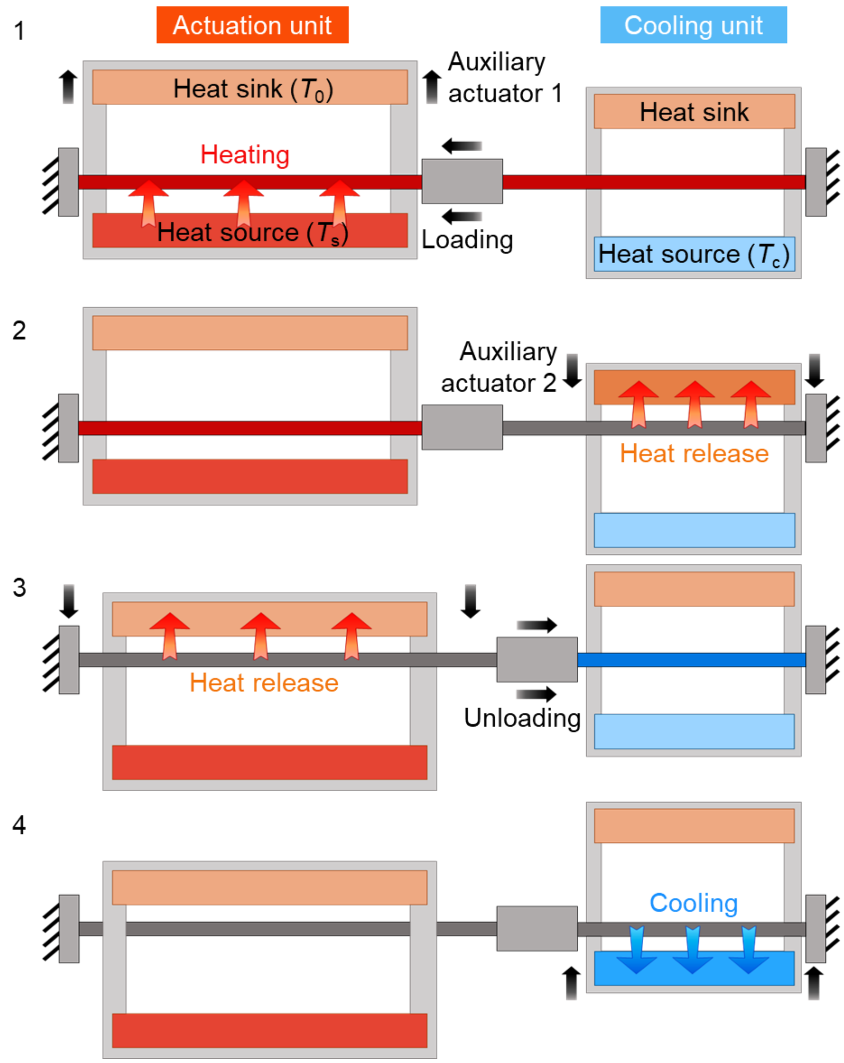

Supplementary Fig. 15. Working principle of the externally heat-driven elastocaloric cooling device. Step 1, The actuator film is heated by the external heat source in the actuation unit through solid–solid contact, generating contraction and loading the refrigerant film, which undergoes stress-induced transformation accompanied by heating. **Step 2,** The refrigerant film contacts the heat sink in the cooling unit and releases heat to the surroundings by conduction. **Step 3,** The actuator film contacts its heat sink and cools back to ambient temperature. The reduced actuation force unloads the refrigerant film, which undergoes the reverse transformation and cools below ambient temperature. **Step 4,** The refrigerant film contacts the heat source in the cooling unit, absorbs heat from the target region, and returns to ambient temperature, completing the cycle.

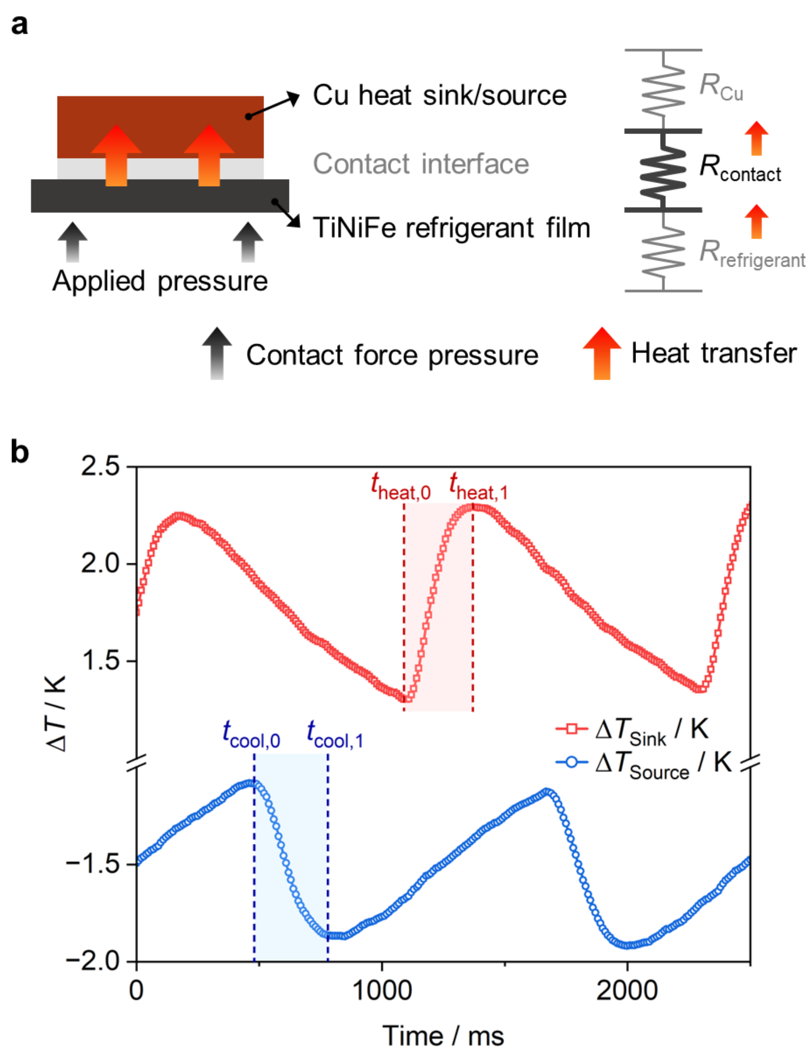

Supplementary Fig. 16. Heat-transfer time between refrigerant film and heat sink/source in the cooling unit. a, Schematic illustration of the heat-transfer pathway from the refrigerant film through the contact interface to the Cu heat sink/source when mechanical pressure is applied. The internal thermal resistances of the refrigerant film ($R_{refrigerant}$) and Cu heat exchanger (R_{Cu}) are assumed negligible due to their small thicknesses and high thermal conductivities, such that the interfacial resistance ($R_{contact}$) dominates the heat-transfer process. **b,** Temperature evolution of the heat sink and heat source during contact with the refrigerant film at 0.83 Hz operation and 500 ms contact duration. The heat sink approaches thermal equilibrium within approximately 270 ms ($t_{heat,0}$ to $t_{heat,1}$), while the heat source requires approximately 350 ms ($t_{cool,0}$ to $t_{cool,1}$). Both values are shorter than the total contact time, indicating sufficient time for effective heat exchange during each cycle. Symbols represent experimental data; lines are guides to the eye.

Supplementary Tables

Supplementary Table 1. Device-level total temperature span ($\Delta T_{total} = T_h - T_c$) and cold-side temperature drop ($\Delta T_c = T_c - T_0$) of the stand-alone elastocaloric cooling unit driven by electromechanical actuators under different boundary conditions, applied strain, and timing parameters. Holding/(un)loading time refers to the duration of thermal contact and mechanical loading/unloading, respectively.

Conditions					
Heat sink	Heat source	Strain ε	Holding/ (Un)loading time (ms)	ΔT_{total} (K)	ΔT_c (K)
Insulated	Insulated	4.0 %	125 / 125	7.2	− 3.5
			250 / 125	6.0	− 3.0
			125 / 250	5.7	− 2.8
			250 / 250	5.1	− 2.6
		4.5 %	125 / 125	8.2	− 3.9
			250 / 125	7.2	− 3.5
			125 / 250	6.6	− 3.2
			250 / 250	6.1	− 3.0
Maintained at T_{amb}	Insulated	4.0 %	125 / 125	5.5	− 4.8
			250 / 125	4.2	− 3.7
			125 / 250	4.1	− 3.6
			250 / 250	3.5	− 3.1
		4.5 %	125 / 125	5.9	− 5.2
			250 / 125	4.7	− 4.1
			125 / 250	4.5	− 4.0
			250 / 250	3.8	− 3.3
Maintained at T_{amb}	Measured with two thermocouples (TC_{mid} position)	4.0 %	125 / 125	–	− 2.9
			250 / 125	–	− 2.8
			125 / 250	–	− 2.4
			250 / 250	–	− 2.3
		4.5 %	125 / 125	–	− 3.3
			250 / 125	–	− 3.1
			125 / 250	–	− 2.6
			250 / 250	–	− 2.6
		4.0 %	125 / 125	–	− 2.8
			250 / 125	–	− 2.7

Measured with two thermocouples (TC_{side} position)		125 / 250	–	− 2.3
		250 / 250	–	− 2.2
	4.5 %	125 / 125	–	− 3.2
		250 / 125	–	− 3.0
		125 / 250	–	− 2.6
		250 / 250	–	− 2.5

Supplementary Table 2. Parameters used for cooling power and specific cooling power calculations.

Parameter	Definition	Value	Unit
ρ_{source}	Density of Cu heat source	8.96 *	$\mathrm{g/cm^3}$
V_{source}	Volume of Cu heat source	0.35 **	$\mathrm{mm^3}$
m_{source}	Mass of Cu heat source	3.14	mg
$c_{\mathrm{p,source}}$	Specific heat capacity of Cu	0.385 *	J/g °C
ρ_{SE}	Density of refrigerant film ($Ti_{49.1}Ni_{50.5}Fe_{0.4}$)	6.46 ***	$\mathrm{g/cm^3}$
V_{SE}	Volume of refrigerant film (active region)	0.098 **	$\mathrm{mm^3}$
m_{SE}	Mass of refrigerant film (active region)	0.630	mg

Footnotes

* Values obtained from literature (see Ref. 2).

** Experimentally measured values.

*** Calculated from nominal atomic composition using atomic weights from Ref. 2.

Supplementary Table 3. Cooling power of Joule-heated and externally heat-driven elastocaloric systems determined by temperature-slope calculation and direct counter-heating measurement.

Actuation mode	$T_c - T_0$ (K)	Cooling power (temperature-slope) (mW)	Cooling power (counter-heating) (mW)
Joule-heated actuation	0	3.08	2.79
	−1	–	1.25
	−1.8	–	0
External heat-source actuation	0	1.36	2.09
	−0.5	–	1.27
	−1.4	–	0

Cooling power determined using the temperature-slope method is derived from the initial temperature decay rate of the heat source under zero temperature lift conditions. Accordingly, values from the temperature-slope method are only provided for $T_c - T_0 = 0$ K. Cooling power determined using the counter-heating method is obtained as described in the Methods section. "–" indicates not applicable.

Supplementary Table 4. Coefficient of performance (COP) and exergetic efficiency of Joule-heated and externally heat-driven elastocaloric systems under different evaluation criteria. Definitions of COP and exergetic efficiency, including the corresponding input-power bases, are provided in Supplementary Note 2. T_0 denotes the ambient temperature, T_c the heat-source temperature in the cooling unit, and T_s the actuator temperature (Joule-heated case) or the external heat-source temperature.

Evaluation conditions		COP	Exergetic efficiency
Joule heating actuation		evaluated at $T_c - T_0 = 0$ K	evaluated at $T_c - T_0 = -1$ K (T_c = 294.3 K) (T_0 = 295.3 K) (T_s = 359.7 K)
Temperature-slope method	Cooler (with work recovery)	5.46	–
	Cooler (without work recovery)	2.88	–
	Thermal actuator efficiency (thermal input basis)	3.27×10^{-2}	–
	Thermal actuator efficiency (electrical input basis)	8.37×10^{-3}	–
	Full system (thermal input basis)	9.43×10^{-2}	–
	Full system (electrical input basis)	2.41×10^{-2}	–
	Full system (thermal input basis + auxiliary actuators)	7.56×10^{-4}	–
	Full system (electrical input basis + auxiliary actuators)	7.39×10^{-4}	–
Counter-heating method	Cooler (with work recovery)	4.94	4.21 %
	Cooler (without work recovery)	2.61	2.22 %
	Thermal actuator efficiency (thermal input basis)	3.27×10^{-2}	3.27 %
	Thermal actuator efficiency (electrical input basis)	8.37×10^{-3}	0.837 %

	Full system (thermal input basis)	8.53×10^{-2}	7.27×10^{-2} %
	Full system (electrical input basis)	2.18×10^{-2}	1.86×10^{-2} %
	Full system (thermal input basis + auxiliary actuators)	6.85×10^{-4}	5.84×10^{-4} %
	Full system (electrical input basis+ auxiliary actuators)	6.69×10^{-4}	5.71×10^{-4} %
External heat-source actuation		evaluated at $T_c - T_0 = 0$ K	evaluated at $T_c - T_0 = -0.5$ K (T_c = 295.1 K) (T_0 = 295.6 K) (T_s = 403.2 K)
Temperature-slope method	Cooler (with work recovery)	2.31	–
	Cooler (without work recovery)	1.50	–
	Thermal actuator efficiency (electrical input basis)	2.43×10^{-3}	–
	Full system (electrical input basis)	3.63×10^{-3}	–
	Full system (electrical input basis+ auxiliary actuators)	2.05×10^{-4}	–
Counter-heating method	Cooler (with work recovery)	3.55	1.37 %
	Cooler without work recovery	2.31	0.892 %
	Thermal actuator efficiency (electrical input basis)	2.43×10^{-3}	0.243 %
	Full system (electrical input basis)	5.60×10^{-3}	2.16×10^{-3} %
	Full system (electrical input basis+ auxiliary actuators)	3.17×10^{-4}	1.22×10^{-4} %

Note:

COP values reported for the full system correspond to the one-way shape memory actuator configuration without work recovery. Values labeled “with work recovery” represent a theoretical upper bound of the cooling unit and are provided for benchmarking future bidirectional actuator designs.

Supplementary Videos

Supplementary Video 1. Operation video of the elastocaloric cooling unit in the Joule-heated coupled heat-driven elastocaloric system.

Supplementary Video 2. Operation video of the thermal actuation unit in the Joule-heated coupled heat-driven elastocaloric system.

Supplementary Video 3. Infrared thermography of the TiNiFe refrigerant film during cyclic operation driven by the Joule-heated thermal actuator.

Supplementary Video 4. Operation video of the thermal actuation unit in the external-heat-source-driven elastocaloric system.

Supplementary Video 5. Operation video of the elastocaloric cooling unit in the external-heat-source-driven elastocaloric system.

Supplementary References

1. ESR Pollmeier GmbH. *Data sheet 6700.161 ML 1 Linearmotoren*. ESR Pollmeier GmbH https://www.esr-pollmeier.de/en/download_documents.php (2012).
2. Rumble, J. R. *CRC Handbook of Chemistry and Physics: A Ready-Reference Book of Chemical and Physical Data*. (CRC Press, Taylor & Francis Group, 2021).